High-resolution range mapping of mycorrhizal fungal species reveals systematic biases in their protection

Authors and affiliations:

1. Qin, Clara (clara@spun.earth): Society for the Protection of Underground Networks, 3500 South Dupont Highway, Suite EI-101, Dover, Delaware 19901, USA
2. Kumar, Sujai: Society for the Protection of Underground Networks, 3500 South Dupont Highway, Suite EI-101, Dover, Delaware 19901, USA
3. Elhance, Jinsu: Society for the Protection of Underground Networks, 3500 South Dupont Highway, Suite EI-101, Dover, Delaware 19901, USA
4. Manley, Bethan F.: Society for the Protection of Underground Networks, 3500 South Dupont Highway, Suite EI-101, Dover, Delaware 19901, USA
5. Corrales, Adriana: Society for the Protection of Underground Networks, 3500 South Dupont Highway, Suite EI-101, Dover, Delaware 19901, USA
6. Polyakov, Anne: Society for the Protection of Underground Networks, 3500 South Dupont Highway, Suite EI-101, Dover, Delaware 19901, USA
7. Stewart, Justin D.: Society for the Protection of Underground Networks, 3500 South Dupont Highway, Suite EI-101, Dover, Delaware 19901, USA; Amsterdam Institute for Life and Environment, Vrije Universiteit, Amsterdam, the Netherlands
8. Kivlin, Stephanie: Department of Ecology and Evolutionary Biology, University of Tennessee, Knoxville, Knoxville, TN 37996, USA
9. Odriozola, Iñaki: Laboratory of Environmental Microbiology, Institute of Microbiology of the Czech Academy of Sciences, Videnska 1083, 14220 Praha 4, Czech Republic
10. Větrovský, Tomáš: Laboratory of Environmental Microbiology, Institute of Microbiology of the Czech Academy of Sciences, Videnska 1083, 14220 Praha 4, Czech Republic
11. Kohout, Petr: Laboratory of Microbial Ecology and Biogeography, Institute of Microbiology of the Czech Academy of Sciences, Czech Republic
12. Baldrian, Petr: Laboratory of Environmental Microbiology, Institute of Microbiology of the Czech Academy of Sciences, Videnska 1083, 14220 Praha 4, Czech Republic
13. Kiers, E. Toby: Society for the Protection of Underground Networks, 3500 South Dupont Highway, Suite EI-101, Dover, Delaware 19901, USA; Amsterdam Institute for Life and Environment, Vrije Universiteit, Amsterdam, the Netherlands
14. Van Nuland, Michael E.: Society for the Protection of Underground Networks, 3500 South Dupont Highway, Suite EI-101, Dover, Delaware 19901, USA

Abstract

Mycorrhizal fungi are essential to ecosystem functioning but have been overlooked in conservation agendas due to data limitations and a historical focus on plants and animals. We present the first global, species-level assessment of the area-based conservation of mycorrhizal fungi. Using 16.5 million site-by-taxon presence–absence records, we created high-resolution range maps for 189 arbuscular mycorrhizal and 2,669 ectomycorrhizal species hypotheses. By intersecting these range maps with protected areas, we show that arbuscular mycorrhizal fungi are less protected than expected by random chance, and both guilds are less protected than terrestrial mammals. We explored the Species Protection Index (SPI) as another conservation metric and found it sensitive to predicted range size. Nonetheless, the SPI framework can be used with our maps to monitor and inform mycorrhizal fungal habitat protection. Our findings highlight the value of species-level spatial data in fungal conservation planning to mitigate extinction risks associated with habitat loss.

Keywords

species conservation, arbuscular mycorrhizal fungi, ectomycorrhizal fungi, terrestrial mammals, Species Protection Index, protected areas, location bias, species distribution modeling, environmental DNA, fungal biogeography

Introduction

The Kunming-Montreal Global Biodiversity Framework aims to conserve 30% of Earth's surface for biodiversity protection (CBD 2022). In contrast to this area-based approach, many conservation frameworks take a species-based approach, including the International Union for Conservation of Nature (IUCN) Red List and the US Endangered Species Act. Because species are distributed unevenly across the Earth's surface, the effectiveness of area-based conservation depends on both the amount and location of protected areas. To maximize the benefits of current and proposed protected areas in conserving the habitat of threatened or endemic species, it is important to incorporate species information into area-based planning [1]. However, nearly all terrestrial species range mapping and subsequent conservation planning are focused on aboveground organisms, whose biodiversity patterns do not serve as reliable proxies for those belowground [2–5].

Soils host 59% of the Earth's species [6], including 2-4 million species of fungi [7]. Among these are mycorrhizal fungi, which form nutrient exchange symbioses with >80% of plant species and receive over 3.5 billion tonnes of carbon from their plant hosts each year [8]. Recent efforts to elucidate the drivers of mycorrhizal fungal biodiversity have revealed distinct community-level spatial patterns that can be used to inform area-based conservation planning [3,4,9–13]. In contrast, species-level spatial modeling of mycorrhizal fungi is still in its infancy: most studies are unable to combine niche predictions with key range-defining mechanisms like dispersal limitation [14–16], leaving many open questions about how climate change and habitat loss translate into species extinction risks. As a result, global conservation status assessments exists for only 805 of the >20,000 described species of ectomycorrhizal fungi [17] and for no

species of arbuscular mycorrhizal fungi [18], even though fungal species face the same primary threats of land use change and climate stress as plants and animals [7].

Our objective was to evaluate the protection of mycorrhizal fungi using two contrasting area-based metrics and in comparison to mammals, which represent a macroscopic and relatively well-studied taxonomic group. We focused our analysis on the two principal guilds of mycorrhizal fungi – arbuscular mycorrhizal (AM) fungi and ectomycorrhizal (EcM) fungi – which differ in their morphology, nutrient acquisition strategy, and host and habitat preferences [19]. We fit species distribution models to the largest databases of fungal environmental DNA (eDNA) sequences ever compiled (Figure 1a), producing the most comprehensive documentation of the geographic distributions of mycorrhizal fungal species to date. Using 2,858 novel mycorrhizal fungal range maps, we conducted the first global-scale estimation of the mycorrhizal fungal Species Protection Index (SPI), which measures the adequacy of the spatial overlap between species ranges and protected area networks [20] (Figure 1b). To complement the SPI, we also implemented a novel statistical test for biases in the location of protected areas relative to mycorrhizal fungal ranges. Because conservation efforts have historically focused on plant and animal diversity [3,21], we hypothesized that mycorrhizal fungal species ranges have a negative protection bias (i.e., have less overlap with current terrestrial protected areas than with a random reshuffling of terrestrial protected areas; Figure 1c). The high-resolution (~1 km^2) range maps resulting from our analyses will allow conservationists to monitor progress in the protection of these critical fungal symbionts, identify priority areas for their protection at sub-national levels, and build a base of knowledge for evaluating species extinction risks associated with habitat loss.

Methods

Species occurrence data

We sourced our species presence–absence records for EcM fungi from GlobalFungi Release 5.0 (https://globalfungi.com/) [22]. These data are a compilation of publicly available ITS amplicon sequences clustered at 97% similarity into operational taxonomic units. Taxonomy was assigned via BLAST against the UNITE 10.0 database [23], and EcM fungal sequences were identified based on genera-level assignments using the FungalTraits database [24]. For AM fungal data, SSU amplicon sequence data from the GlobalAMFungi database was used [25]. Taxonomy was assigned to SSU amplicons via BLAST against MaarjAM database virtual taxa [26]. These databases represent the largest collection of fungal eDNA sequence data to date. Because the minimum resolution of our covariate rasters was 30 arc-seconds (~1 km^2 at the equator) in the World Geodetic System 1984 (WGS84) projection, we spatially aggregated soil samples in each database into a grid cell of this resolution to produce new observational units hereafter referred to as “sites.”

Species range maps

We modeled the distribution of each AM fungal virtual taxon and EcM fungal operational taxonomic unit (hereafter referred to generically as “species hypotheses”) present in at least 31 sites using Hierarchical Modelling of Species Communities (HMSC) [27] via the *Hmsc* R package

[28] and the *Hmsc-hpc* Python package [29]. Briefly, HMSC is a Bayesian framework for species distribution modeling that uses spatial latent factors to account for the influence of processes not captured by the covariates (e.g., dispersal limitation, missing environmental variables, and species interactions). These latent factors are modeled to be spatially autocorrelated, so that closer sites are more similar [27]. Our covariates included climate [30,31], soil [32,33], vegetation [34](Running and Zhao, 2019), and technical variables outlined in Table S1. All spatial covariate layers were reprojected and resampled to a unified grid in WGS84 at 30 arc-second resolution. Finally, using Google Earth Engine [35] via the *rgee* R package [36], we predicted each species hypothesis' probability of presence at each grid cell on Earth's terrestrial surface for which raster layer data were available for all predictors (Figure 1d).

We modeled the distributions of AM fungi jointly, using the spatial latent factors in HMSC to capture co-occurrence patterns between AM fungal virtual taxa. By contrast, we modeled the relatively endemic distributions of EcM fungi independently of each other, as capturing the co-occurrence patterns of such highly endemic taxa would require more latent factors than memory constraints allow. (See Supplementary Text S1 for more details on model fitting, evaluation, and prediction.) For both guilds, we defined the range as the collection of grid cells in which the probability of presence exceeds 1%. This threshold, while low, is intended to reduce the number of zero-range-size species hypotheses that would be excluded from our analysis, and increasing the threshold does not qualitatively change our key metrics (Table S2). We also downloaded preexisting specimen-based range maps for all 6,226 terrestrial mammal species [37] (Map of Life 2021).

Species Protection Index

Given a collection of species, the SPI is calculated as an endemism-weighted mean of individual species-level metrics called Species Protection Scores. These range from 0 to 100 in a linear relationship with the proportion protected of the species' total range, where a score of 100 represents a proportion equal to or greater than the species' representation target. These representation targets are determined based on the reasoning that, due to the increased risk of extinction for smaller populations, rare and endemic species should require a greater proportion of their range to be protected than cosmopolitan species (Figure 1b). The SPI attempts to quantify conservation progress based on this heuristic, rather than using precise extinction–area curves for each species, which can be difficult to define. We calculated the SPI following the methods of Jetz et al. (2021) except that representation targets were not capped at an upper limit. We utilized all polygons in the World Database of Protected Areas (UNEP-WCMC and IUCN 2025).

Protection bias

To assess bias in the location of protected areas relative to species ranges, which we call "protection bias," we compared the proportion of species ranges overlapping with protected areas to the proportion expected under null expectations (Figure 1c). Namely, after a random reshuffling of total terrestrial protected area, the proportion protected of a species range is expected to be equal to the proportion protected of Earth's terrestrial surface [38]. Furthermore, as the species' geographic range size increases, the difference between the proportions protected in the observed and null cases is expected to scale by the inverse of the square root of the

range size. We developed a protection bias statistic B_i to measure and standardize this difference across species with variable range sizes:

$$B_i = \mathrm{sqrt}(a_i) * (p_i - mu)$$

where a_i is the range size of species i in km^2, p_i is the proportion protected of the range of species i, and mu is the proportion protected of Earth's land surface excluding Antarctica (~0.173).

By ignoring potential phylogenetic autocorrelation in the geographic distributions of species, we assumed that B_i are independently and identically distributed with a zero-centered probability distribution under null expectations. With the central limit theorem, it is straightforward to calculate the mean B_i and its standard error for each taxonomic group. This makes it possible to test whether the mean observed protection bias within each taxonomic group is lower or higher than expected (zero). The test is equivalent to comparing the weighted mean p_i to mu, so p_i are reported instead of B_i for the global-scale analysis.

We also calculated the biome-level protection biases for AM and EcM fungi (Supplementary Text S2). We conducted the biome-level analysis for all biomes in the RESOLVE dataset [39] except for mangroves due to their relatively small area. Because Antarctica is excluded from our analysis, we also ignored Antarctic tundra.

Results

We created range maps for 189 of roughly 332 formally described AMF virtual taxa [40](Schüßler and Walker 2024) and 2,669 EcM fungal operational taxonomic units spanning 226 of all 308 defined EcM fungal genera [17]. The presence–absence data for these AM and EcM fungal species come from 512 and 6,158 sites, respectively, forming a dataset of 16,532,470 site-by-species-hypothesis presence–absence records. Across AM and EcM fungal models, cross-validation error did not vary with predicted range protection (Figure S1). This suggests that our results are robust to model performance. Estimates of cross-validation error are reported in Table S3.

Species Protection Index

We found that at the global level, the SPI is highest for AM fungi, intermediate for EcM fungi, and lowest for terrestrial mammals (Table 1). At the country level, the SPI for AM and EcM fungi are positively correlated (r = 0.84) but not strictly coupled, differing by more than 40 points in at least 12 countries (Table S4). At the subnational level, we demonstrate how an SPI analysis using mycorrhizal fungal species range maps can inform future protected area locations (Box 1). As an index, however, the SPI is sensitive to the assumptions used to define a species' representation target as a function of its total range size (Table 1). Therefore, it may not be well-suited for AM fungi given ongoing questions about species delimitations that impact species-level endemism patterns [41–43].

Protection bias

Relative to the random-chance expectation that species ranges are protected in equal proportion to Earth's terrestrial surface (~0.173; UNEP-WCMC and IUCN 2025), we found AM

fungi have a negative protection bias (weighted mean proportion protected ± weighted SE: $0.147 \pm 1.6*10^{-4}$). In contrast, EcM fungi ($0.180 \pm 3.9*10^{-5}$) and mammals ($0.206 \pm 2.0*10^{-5}$) have a positive protection bias (Figure 2, Table S5). Biome-level analyses of protection bias provide insight into the drivers of global protection biases (Figure 3).

For AM fungi, the relative shares of species ranges across biomes (Figure 3a) and the proportions protected of each biome's total land area (Figure 3b) lead temperate grasslands to have the strongest negative contribution to the global protection bias (Figure 3c). While this is likely driven by the biome's strong representation of croplands, which typically deter protected areas [44], AM fungi have a negative protection bias at the global level even when croplands are removed from the analysis (Table S5).

For EcM fungi, boreal forests contribute the strongest negative bias (Figure 3f), due to the large shares of EcM fungal species ranges within this biome (Figure 3d) and the under-protection of this biome relative to the global terrestrial baseline (Figure 3e). However, this is outweighed by the strong positive contribution from temperate broadleaf forests (Figure 3f), where EcM fungi are both highly concentrated (Figure 3d) and receive above-average protection at both the global and biome level (Figure 3e).

Discussion

We developed a novel set of global high-resolution range maps spanning 2,858 species hypotheses of AM and EcM fungi to establish a baseline for their area-based protection. Using these range maps, we quantified the SPI and the protection bias for mycorrhizal fungi at multiple spatial scales to demonstrate their utility for conservation planning in diverse decision-making contexts [45].

The SPI and protection bias analyses yielded contrasting results. The SPI suggests that AM fungi are well protected, while EcM fungi and terrestrial mammals are only moderately protected. In contrast, our protection bias analysis indicates that AM fungi are less protected than expected by random chance, while EcM fungi and terrestrial mammals are more protected than expected. While these methods complement one another, we argue that the protection bias is a more appropriate metric for the area-based protection of mycorrhizal fungi given the current state of knowledge. The SPI assumes a relationship between range size and extinction risk that is not yet validated for fungi [46]. Additionally, the SPI systematically favors taxa with large range sizes: as range size increases, the representation target required under default assumptions decreases from 100% to 15% of the species' total range size, while the proportion protected of the species' total range tends towards the global terrestrial baseline (~17.3%, excluding Antarctica). Thus, the higher SPI of AM fungi is mostly driven by their large range sizes rather than their association with protected areas. Although our range size estimates for AM fungi are in line with previous estimates [47], the virtual taxa used in these estimates have been criticized for relying on a conservative species delimitation that may inflate range sizes [42]. A finer-scale delimitation may better accommodate the complexities of AM fungal genetics, including their coenocytic nature. This would enable a closer examination of endemism in this guild [43] and a more robust foundation for calculating the SPI.

Consistent with prior findings [38], we show that terrestrial mammals are better protected than expected by random chance. In this context, the worse-than-random protection of AM fungal ranges adds to a growing body of evidence that fungal biodiversity patterns do not necessarily align with those used to delineate ecoregions [2,48] or inform protected area planning [4,5], with the possible exception of EcM fungi [49]. EcM fungal ranges are better protected than by random chance, but less well protected than terrestrial mammal ranges. While EcM fungal protection is higher in temperate broadleaf forests, it falls short in two critical biomes: boreal forests and tropical moist forests. The lower-than-random protection of EcM fungal ranges in tropical moist forests is striking, given the greater-than-random share of protected area in this biome. It also contrasts with recent predictions that community-level rarity hotspots of tropical EcM fungi have strong overlaps with protected areas [4]. One potential explanation for this discrepancy is that it results from the exclusion of tropical rare species from our range maps due to insufficient presences in the occurrence records; however, this explanation would also require a negative relationship between the number of presences and protection, which is not apparent in our data (Figure S2). Thus, this finding supports the view that community-level metrics may obscure species-level patterns important for conservation planning.

The IUCN Red List, the global authority on species conservation statuses, assesses fungi by inferring their geographic ranges and population trends from sporocarp observations [46]. For the many species that do not produce sporocarps, including all AM fungi, our range maps offer one of the few sources of information on these species' distributions. For species that produce sporocarps, however, we acknowledge that there remain some obstacles to using our range maps for red-listing. First, the probability of presence of a species is not coupled to its population size [50], so our range maps primarily inform those IUCN criteria related to geographic distribution. Second, the short-read sequencing technologies commonly used in fungal eDNA surveys, including those compiled in the GlobalFungi databases, may be unable to differentiate closely related species. The resulting ambiguity prevents eDNA records from being readily combined with sporocarp records for conservation assessments. These obstacles may be partially overcome by carefully cross-validating eDNA-based and sporocarp-based data. In particular, the increased taxonomic resolution offered by long-read sequencing technologies may enable more confident taxonomic assignments [51], which can then be validated against sporocarp presence and abundance in well-sampled regions.

Species-level modeling of mycorrhizal fungal biodiversity has begun to fill a critical gap left by community-level modeling: the translation of habitat loss into extinction risk. While extinction outcomes ultimately depend on many factors, our range maps serve as an initial base of knowledge, enabling quantitative tools like the Species Protection Index to estimate fungal species' conservation statuses and evaluate competing protected area arrangements. Future research should examine mycorrhizal plant–fungal range dynamics to better understand the reciprocal impacts of plant and fungal protections, especially in the face of climate change. We contend that conservation strategies should direct more attention to mycorrhizal fungal distributions to address species protection biases, and we believe that range mapping efforts such as the one initiated here represent an important step towards achieving this goal.

Boxes

Box 1. Using ectomycorrhizal fungal species range maps for conservation monitoring and decision support.

Because little was known about the spatial distribution of belowground biodiversity until recently, area-based conservation planning has necessarily been more informed by the distribution of aboveground biodiversity. Our high-resolution range maps for mycorrhizal fungal species provide a knowledge base to steer conservation towards equitable consideration of belowground biodiversity. This makes it possible to monitor progress towards species conservation targets and to support decision-making about the location of future protected areas.

Monitoring. We can overlay our mycorrhizal fungal species range maps with historical data on the spatial distribution of protected areas to compare country-level changes in the EcM fungal SPI across time. For example, Chile and Finland had similar amounts of protected land area by percentage of their total land areas in 2020 (Chile: 27.9%; Finland: 20.5%) and increased their protected area networks by a similar proportion of their respective land areas between 2020 and 2025 (Chile: +0.8%; Finland: +0.7%). Nonetheless, Chile saw a much smaller increase in its EcM fungal SPI than did Finland (Chile: +0.5; Finland +4.4).

Decision support. We can use species range maps to reveal the optimal locations of future protected areas for EcM fungal conservation. Figure X displays heatmaps of the potential SPI gains associated with the hypothetical addition of protected areas in Chile and Finland as of January 2020. Hotspots are areas with a high concentration of endemic species. These heatmaps are juxtaposed against the actual distribution of protected areas established between January 2020 and January 2025. While Chile's recent protected areas were concentrated in coldspots, culminating in minimal gains in SPI, Finland's recent protected areas were distributed relatively evenly across its landmass, culminating in intermediate gains in SPI. Moving forward, heatmaps of potential SPI gains can be consulted alongside other pragmatic considerations to determine the best locations for new protected areas.

Acknowledgments

Society for the Protection of Underground Networks (SPUN) is supported by grants from the Jeremy and Hannelore Grantham Environmental Trust, Paul Allen Family Foundation, the Schmidt Family Foundation, Quadrature Climate Foundation, and the Bezos Earth Fund. ETK acknowledges support from NWO-VICI (202.012), NWO-Spinoza (SPI.2023.2) and HFSP (RGP 0029). TV and PK acknowledge support from the Czech Science Foundation (21-17749S). PB acknowledges support from MEYS CR (LC23152, LM2023055).

Data Availability Statement

All code used for analysis will be made publicly available on a digital repository upon acceptance of this manuscript.

Conflict of Interest Statement

ETK is a co-founder of the Society for the Protection of Underground Networks (SPUN), a non-governmental organization that conducts research on mycorrhizal fungi for conservation and restoration.

Tables

Table 1. Range sizes and global Species Protection Indices (SPI) of mycorrhizal fungi and terrestrial mammals at various representation target levels [†].

Taxonomic group	No. taxa analyzed	Range size (thousands of km^2), median (5^{th} – 95^{th} percentiles)	Global SPI, mean ± SE, assuming representation target declines to percentage *p* of total range size as range size increases		
			p = 15% (default)	*p* = 30%	*p* = 100%
Arbuscular mycorrhizal fungi	189	40,378 (14,205 – 77,975)	88.49 ± 1.16	48.10 ± 0.88	14.43 ± 0.26
Ectomycorrhizal fungi	2,669	256 (<1 – 5,081)	69.26 ± 0.65	49.39 ± 0.53	21.88 ± 0.31
Terrestrial mammals	6,226	168 (3 – 6,567)	61.09 ± 0.45	47.02 ± 0.39	22.68 ± 0.23

[†] When species with large range sizes are assumed to require a protected area equivalent to 30% instead of 15% of their total range size, holding all other assumptions constant, the global SPI declines across all taxonomic groups to similar values. When the representation target for large range-sized species is further increased to 100%, the SPI further declines across all taxonomic groups and becomes highest for terrestrial mammals, intermediate for ectomycorrhizal fungi, and lowest for arbuscular mycorrhizal fungi.

Figures

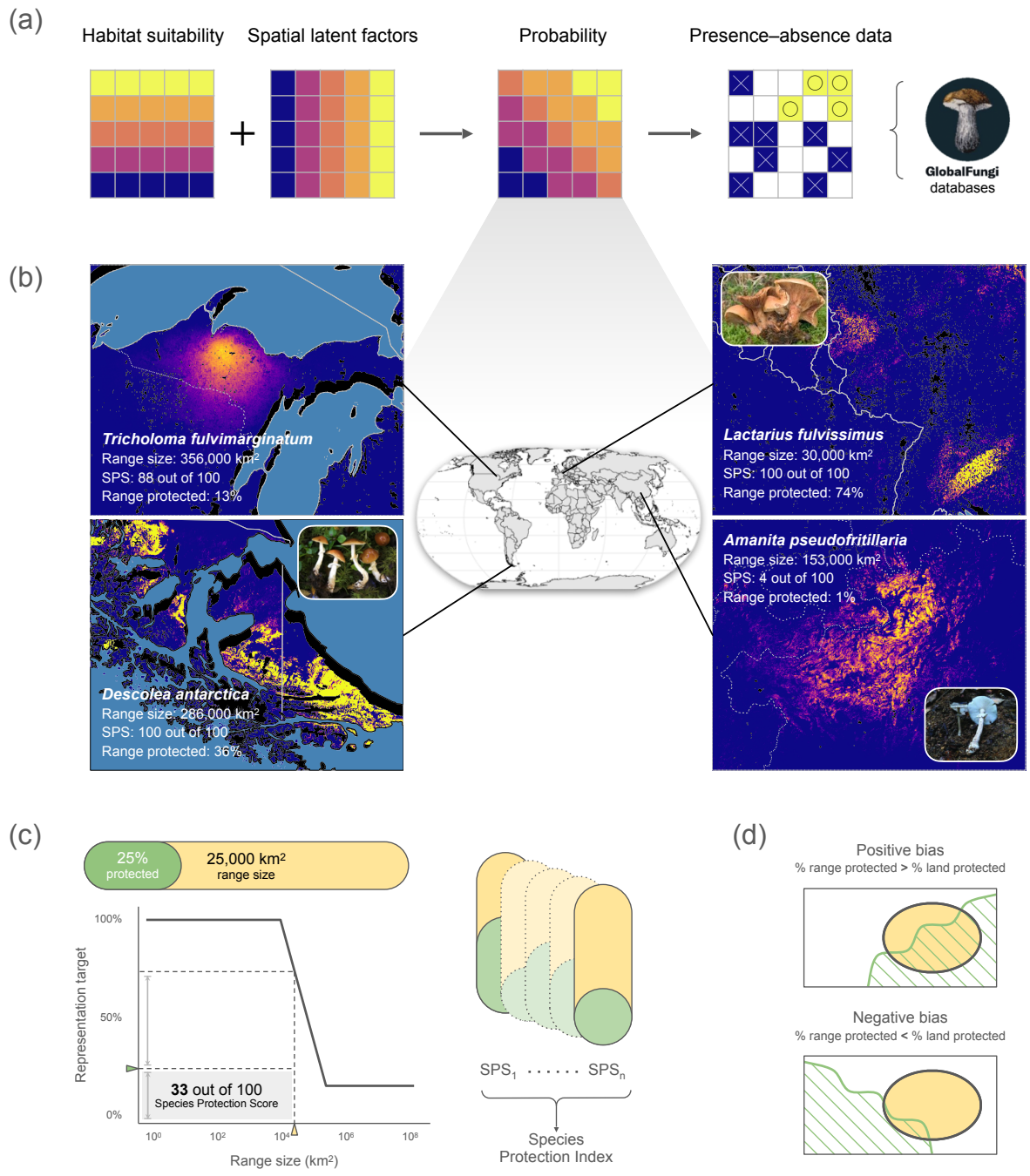

Figure 1. Conceptual overview of the analysis and examples of model predictions. (a) To generate mycorrhizal fungal species range maps, we compiled georeferenced fungal genomic data from the GlobalFungi and GlobalAMFungi databases and environmental data from a collection of 1 km^2-scale global raster layers. We ingested this data in a Bayesian spatial latent factor model and used the fitted model with the raster layers to make predictions of each species' probability of presence across Earth's terrestrial surface excluding Antarctica. (b)

Predicted distributions for four example EcM fungal species hypotheses, represented by sequences with > 99% match to the corresponding species' UNITE reference sequences. Each inset map displays a heatmap of the probability of presence (blue to yellow, 0% to 100%) across an area of approximately 500 km by 400 km. Made with Natural Earth using the *rnaturalearth* R package [52]. Photo credits: *A. pseudofritillaria*, modified from [53]; *D. antarctica*, M. E. Smith, https://redlist.info/iucn/species_view/296578; *L. fulvissimus*, CC BY-SA 3.0 amadej trnkoczy on Mushroom Observer, https://mushroomobserver.org/images/107090?q=25oLo. (c) We calculated the Species Protection Index (SPI) for arbuscular mycorrhizal (AM) fungi, ectomycorrhizal (EcM) fungi, and terrestrial mammals at the global level. Briefly, this entails calculating the representation target for each species based on a function of its range size; calculating each species' area of overlap with protected areas to quantify, using the Species Protection Score (SPS), its progress towards its representation target; and taking the mean across species in the taxonomic group. Here, hypothetical species ranges are displayed as examples. (d) Species protection biases can be negative or positive depending on whether the proportion of the species range (yellow ellipse) intersecting with protected areas (green single-hatched region) is less than or greater than the proportion protected of total land area.

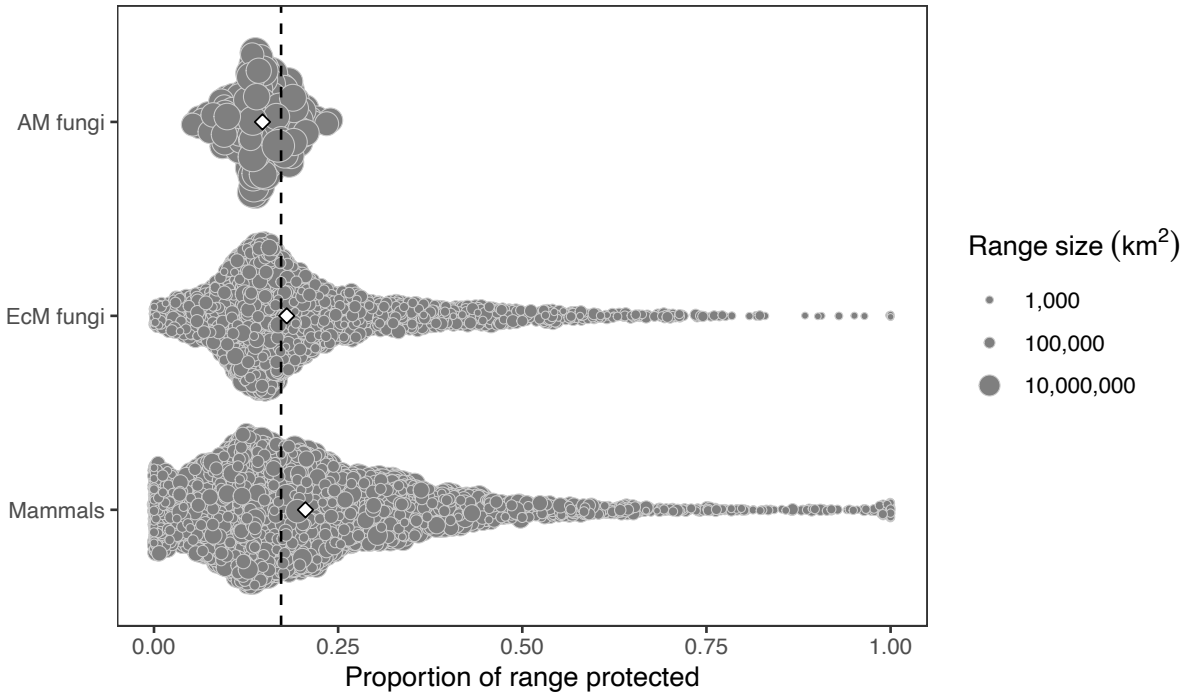

Figure 2. Proportions protected of species ranges across taxonomic groups at the global level. The global protection bias is quantified by comparing the weighted mean (diamonds) proportions protected of species' ranges (circles) to the expected proportion protected under random chance (dotted line), where weights are given by the square root of the range size (size of circles). Error bars are not displayed because the upper and lower bars visually overlap even at 99.9% confidence. Antarctica is excluded from this analysis. Abbreviations: AM, arbuscular mycorrhizal; EcM, ectomycorrhizal.

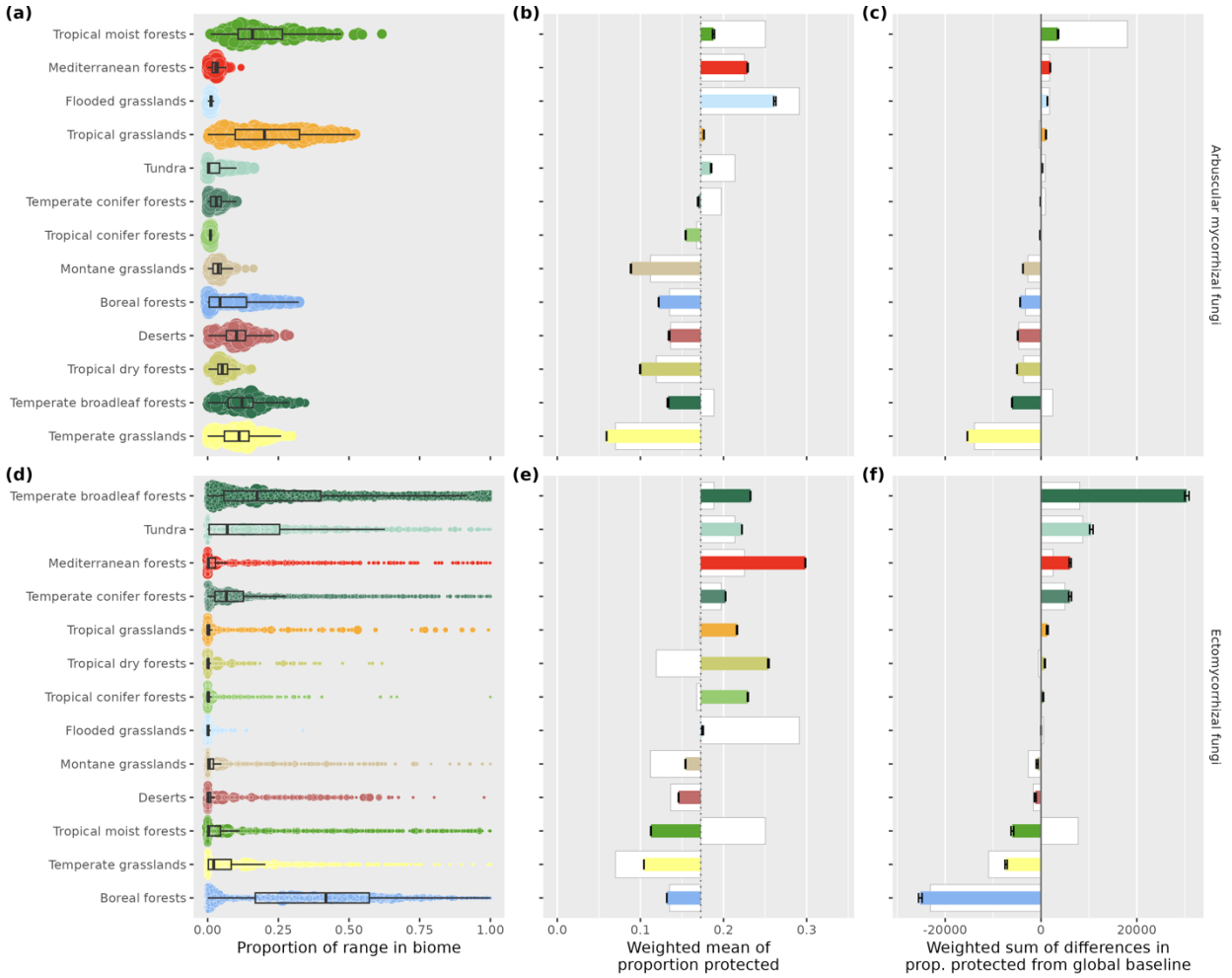

Figure 3. Protection biases of mycorrhizal fungal species ranges across terrestrial biomes. (a,d) Proportions of species ranges (circles) falling within each biome. Boxplots summarize the proportions weighted by the square roots of the corresponding species' global range sizes (circle sizes). The "range-size weight" is the proportion of the species' range within each biome multiplied by the square root of the species' global range size. (b,e) Range-size-weighted mean proportions protected of within-biome species ranges (error-barred ends of colored bars), relative to the global-level proportion protected (vertical dotted line) and the biome-level proportions protected (white bars). (c,f) The unitless contribution of a biome's protected area network to a taxonomic group's global protection bias (colored bars) is quantified by the range-size-weighted sum of the differences between the proportions protected of species ranges and the proportion protected of global land area (i.e. the dot product of the left-hand column with the middle column). More-positive (versus more-negative) values denote that the spatial distribution of protected areas within the biome contributes more positively (versus more negatively) to the corresponding taxonomic group's global protection bias. Values of zero denote a net-zero contribution within the biome to the global protection bias. White bars represent the hypothetical biome-level contributions had all species been protected at parity with the biome in which they were found. Differences between biomes in the proportion of area protected explain 51–87% of the global protection bias of AM fungi and only 19–20% of the global protection bias of EcM

fungi. In the two right-hand columns, error bars represent 99.9% confidence intervals. Antarctica is excluded from this analysis.

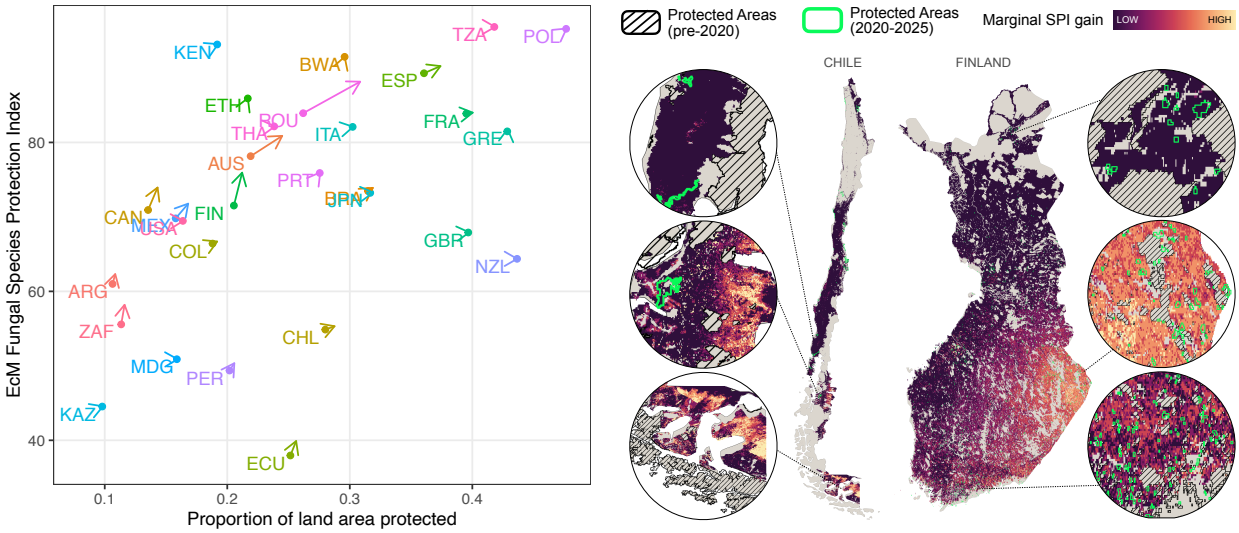

(Box 1) Figure X. Comparison of the changes in Species Protection Index (SPI) for ectomycorrhizal (EcM) fungi associated with new protected areas across a selection of countries. The arrow plot displays the change in SPI and the change in the proportion of land area protected for each country (labeled by ISO 3166 standard codes) between January 2020 and January 2025. The maps highlight changes in Chile (CHL) versus Finland (FIN) over this period. This version of the SPI assumes default parameters, i.e. that the representation target declines to 15% with increasing range size. Made with Natural Earth using the *rnaturalearth* R package [52].

References

CBD (2022). COP Decision 15/4. *Kunming-Montreal Global Biodiversity Framework*. Available at: https://www.cbd.int/doc/decisions/cop-15/cop-15-dec-04-en.pdf

Running, S., and Zhao, M. (2019). *MOD17A3HGF MODIS/Terra Net Primary Production Gap-Filled Yearly L4 Global 500 m SIN Grid V006* [Data set]. NASA Land Processes Distributed Active Archive Center. https://doi.org/10.5067/MODIS/MOD17A3HGF.006 Date Accessed: 2025-07-13

Map of Life. (2021). Mammal range maps harmonised to the Mammals Diversity Database [Data set]. Map of Life. https://doi.org/10.48600/MOL-48VZ-P413

UNEP-WCMC and IUCN (2025), Protected Planet: The World Database on Protected Areas (WDPA) [On-line], January 2025, Cambridge, UK: UNEP-WCMC and IUCN Available at: www.protectedplanet.net.

Schüßler, A., and Walker, C. 2024. Glomeromycota Phylogeny. http://www.amf-phylogeny.com/

1. Langhammer, P. F., Bull, J. W., Bicknell, J. E., Oakley, J. L., Brown, M. H., Bruford, M. W., Butchart, S. H. M., Carr, J. A., Church, D., Cooney, R., Cutajar, S., Foden, W., Foster, M. N., Gascon, C., Geldmann, J., Genovesi, P., Hoffmann, M., Howard-McCombe, J., Lewis, T., Macfarlane, N. B. W., Melvin, Z. E., Merizalde, R. S., Morehouse, M. G., Pagad, S., Polidoro, B., Sechrest, W., Segelbacher, G., Smith, K. G., Steadman, J., Strongin, K., Williams, J., Woodley, S. & Brooks, T. M. The positive impact of conservation action. *Science* **384**, 453–458 (2024).
2. Vasar, M., Davison, J., Sepp, S., Mucina, L., Oja, J., Al-Quraishy, S., Anslan, S., Bahram, M., Bueno, C. G., Cantero, J. J., Decocq, G., Fraser, L., Hiiesalu, I., Hozzein, W. N., Koorem, K., Meng, Y., Moora, M., Onipchenko, V., Öpik, M., Pärtel, M., Vahter, T., Tedersoo, L., Zobel, M. & Soininen, J. Global soil microbiomes: A new frontline of biome-ecology research. *Glob. Ecol. Biogeogr.* geb.13487 (2022) doi:10.1111/geb.13487.

3. Guerra, C. A., Berdugo, M., Eldridge, D. J., Eisenhauer, N., Singh, B. K., Cui, H., Abades, S., Alfaro, F. D., Bamigboye, A. R., Bastida, F., Blanco-Pastor, J. L., De Los Ríos, A., Durán, J., Grebenc, T., Illán, J. G., Liu, Y.-R., Makhalanyane, T. P., Mamet, S., Molina-Montenegro, M. A., Moreno, J. L., Mukherjee, A., Nahberger, T. U., Peñaloza-Bojacá, G. F., Plaza, C., Picó, S., Verma, J. P., Rey, A., Rodríguez, A., Tedersoo, L., Teixido, A. L., Torres-Díaz, C., Trivedi, P., Wang, J., Wang, L., Wang, J., Zaady, E., Zhou, X., Zhou, X.-Q. & Delgado-Baquerizo, M. Global hotspots for soil nature conservation. *Nature* **610**, 693–698 (2022).
4. Van Nuland, M. E., Averill, C., Stewart, J. D., Prylutskyi, O., Corrales, A., van Galen, L. G., Manley, B. F., Qin, C., Lauber, T., Mikryukov, V., Dulia, O., Furci, G., Marín, C., Sheldrake, M., Weedon, J. T., Peay, K. G., Cornwallis, C. K., Větrovský, T., Kohout, P., Baldrian, P., Tedersoo, L., West, S. A., Crowther, T. W., Kiers, E. T. & van den Hoogen, J. Global hotspots of mycorrhizal fungal richness are poorly protected. *Nature* 1–9 (2025) doi:10.1038/s41586-025-09277-4.
5. Van Galen, L. G., Stewart, J. D., Qin, C., Corrales, A., Manley, B. F., Kiers, E. T., Crowther, T. W. & Van Nuland, M. E. Global divergence in plant and mycorrhizal fungal diversity hotspots. *Nat. Commun.* **16**, 6702 (2025).
6. Anthony, M. A., Bender, S. F. & van der Heijden, M. G. A. Enumerating soil biodiversity. *Proc. Natl. Acad. Sci.* **120**, e2304663120 (2023).
7. Niskanen, T., Lücking, R., Dahlberg, A., Gaya, E., Suz, L. M., Mikryukov, V., Liimatainen, K., Druzhinina, I., Westrip, J. R. S., Mueller, G. M., Martins-Cunha, K., Kirk, P., Tedersoo, L. & Antonelli, A. Pushing the Frontiers of Biodiversity Research: Unveiling the Global Diversity, Distribution, and Conservation of Fungi. *Annu. Rev. Environ. Resour.* **48**, 149–176 (2023).
8. Hawkins, H.-J., Cargill, R. I. M., Van Nuland, M. E., Hagen, S. C., Field, K. J., Sheldrake, M., Soudzilovskaia, N. A. & Kiers, E. T. Mycorrhizal mycelium as a global carbon pool. *Curr. Biol.* **33**, R560–R573 (2023).

9. Kivlin, S. N., Hawkes, C. V. & Treseder, K. K. Global diversity and distribution of arbuscular mycorrhizal fungi. *Soil Biol. Biochem.* **43**, 2294–2303 (2011).
10. van der Linde, S., Suz, L. M., Orme, C. D. L., Cox, F., Andreae, H., Asi, E., Atkinson, B., Benham, S., Carroll, C., Cools, N., De Vos, B., Dietrich, H.-P., Eichhorn, J., Gehrmann, J., Grebenc, T., Gweon, H. S., Hansen, K., Jacob, F., Kristöfel, F., Lech, P., Manninger, M., Martin, J., Meesenburg, H., Merilä, P., Nicolas, M., Pavlenda, P., Rautio, P., Schaub, M., Schröck, H.-W., Seidling, W., Šrámek, V., Thimonier, A., Thomsen, I. M., Titeux, H., Vanguelova, E., Verstraeten, A., Vesterdal, L., Waldner, P., Wijk, S., Zhang, Y., Žlindra, D. & Bidartondo, M. I. Environment and host as large-scale controls of ectomycorrhizal fungi. *Nature* **558**, 243–248 (2018).
11. Větrovský, T., Kohout, P., Kopecký, M., Machac, A., Man, M., Bahnmann, B. D., Brabcová, V., Choi, J., Meszárošová, L., Human, Z. R., Lepinay, C., Lladó, S., López-Mondéjar, R., Martinović, T., Mašínová, T., Morais, D., Navrátilová, D., Odriozola, I., Štursová, M., Švec, K., Tláskal, V., Urbanová, M., Wan, J., Žifčáková, L., Howe, A., Ladau, J., Peay, K. G., Storch, D., Wild, J. & Baldrian, P. A meta-analysis of global fungal distribution reveals climate-driven patterns. *Nat. Commun.* **10**, 1–9 (2019).
12. Steidinger, B. S., Bhatnagar, J. M., Vilgalys, R., Taylor, J. W., Qin, C., Zhu, K., Bruns, T. D. & Peay, K. G. Ectomycorrhizal fungal diversity predicted to substantially decline due to climate changes in North American Pinaceae forests. *J. Biogeogr.* 1–11 (2020) doi:10.1111/jbi.13802.
13. Mikryukov, V., Dulya, O., Zizka, A., Bahram, M., Hagh-Doust, N., Anslan, S., Prylutskyi, O., Delgado-Baquerizo, M., Maestre, F. T., Nilsson, H., Pärn, J., Öpik, M., Moora, M., Zobel, M., Espenberg, M., Mander, Ü., Khalid, A. N., Corrales, A., Agan, A., Vasco-Palacios, A.-M., Saitta, A., Rinaldi, A., Verbeken, A., Sulistyo, B., Tamgnoue, B., Furneaux, B., Duarte Ritter, C., Nyamukondiwa, C., Sharp, C., Marín, C., Gohar, D., Klavina, D., Sharmah, D., Dai, D.-Q., Nouhra, E., Biersma, E. M., Rähn, E., Cameron, E., De Crop, E., Otsing, E., Davydov,

E., Albornoz, F., Brearley, F., Buegger, F., Zahn, G., Bonito, G., Hiiesalu, I., Barrio, I., Heilmann-Clausen, J., Ankuda, J., Doležal, J., Kupagme, J., Maciá-Vicente, J., Djeugap Fovo, J., Geml, J., Alatalo, J., Alvarez-Manjarrez, J., Põldmaa, K., Runnel, K., Adamson, K., Bråthen, K.-A., Pritsch, K., Tchan Issifou, K., Armolaitis, K., Hyde, K., Newsham, K. K., Panksep, K., Lateef, A. A., Hansson, L., Lamit, L., Saba, M., Tuomi, M., Gryzenhout, M., Bauters, M., Piepenbring, M., Wijayawardene, N. N., Yorou, N., Kurina, O., Mortimer, P., Meidl, P., Kohout, P., Puusepp, R., Drenkhan, R., Garibay-Orijel, R., Godoy, R., Alkahtani, S., Rahimlou, S., Dudov, S., Põlme, S., Ghosh, S., Mundra, S., Ahmed, T., Netherway, T., Henkel, T., Roslin, T., Nteziryayo, V., Fedosov, V., Onipchenko, V., Yasanthika, W. A. E., Lim, Y., Van Nuland, M., Soudzilovskaia, N., Antonelli, A., Kõljalg, U., Abarenkov, K. & Tedersoo, L. Connecting the multiple dimensions of global soil fungal diversity. *Sci. Adv.* **9**, eadj8016 (2023).

14. Davison, J., Moora, M., Semchenko, M., Adenan, S. B., Ahmed, T., Akhmetzhanova, A. A., Alatalo, J. M., Al-Quraishy, S., Andriyanova, E., Anslan, S., Bahram, M., Batbaatar, A., Brown, C., Bueno, C. G., Cahill, J., Cantero, J. J., Casper, B. B., Cherosov, M., Chideh, S., Coelho, A. P., Coghill, M., Decocq, G., Dudov, S., Fabiano, E. C., Fedosov, V. E., Fraser, L., Glassman, S. I., Helm, A., Henry, H. A. L., Hérault, B., Hiiesalu, I., Hiiesalu, I., Hozzein, W. N., Kohout, P., Kõljalg, U., Koorem, K., Laanisto, L., Mander, Ü., Mucina, L., Munyampundu, J. P., Neuenkamp, L., Niinemets, Ü., Nyamukondiwa, C., Oja, J., Onipchenko, V., Pärtel, M., Phosri, C., Põlme, S., Püssa, K., Ronk, A., Saitta, A., Semboli, O., Sepp, S. K., Seregin, A., Sudheer, S., Peña-Venegas, C. P., Paz, C., Vahter, T., Vasar, M., Veraart, A. J., Tedersoo, L., Zobel, M. & Öpik, M. Temperature and pH define the realised niche space of arbuscular mycorrhizal fungi. *New Phytol.* **231**, 763–776 (2021).
15. Kivlin, S. N., Hawkes, C. V., Papeş, M., Treseder, K. K. & Averill, C. The future of microbial ecological niche theory and modeling. *New Phytol.* **231**, 508–511 (2021).

16. Van Nuland, M. E., Qin, C., Pellitier, P. T., Zhu, K. & Peay, K. G. Climate mismatches with ectomycorrhizal fungi contribute to migration lag in North American tree range shifts. *Proc. Natl. Acad. Sci.* **121**, e2308811121 (2024).
17. Van Galen, L. G., Corrales, A., Truong, C., Hoogen, J. van den, Kumar, S., Manley, B. F., Stewart, J. D., Kohout, P., Baldrian, P., Větrovský, T., Crowther, T. W., Kiers, E. T. & Van Nuland, M. E. The biogeography and conservation of Earth's 'dark' ectomycorrhizal fungi. *Curr. Biol.* **35**, R563–R574 (2025).
18. Mueller, G. M., Cunha, K. M., May, T. W., Allen, J. L., Westrip, J. R. S., Canteiro, C., Costa-Rezende, D. H., Drechsler-Santos, E. R., Vasco-Palacios, A. M., Ainsworth, A. M., Alves-Silva, G., Bungartz, F., Chandler, A., Gonçalves, S. C., Krisai-Greilhuber, I., Iršėnaitė, R., Jordal, J. B., Kosmann, T., Lendemer, J., McMullin, R. T., Mešić, A., Motato-Vásquez, V., Ohmura, Y., Næsborg, R. R., Perini, C., Saar, I., Simijaca, D., Yahr, R. & Dahlberg, A. What Do the First 597 Global Fungal Red List Assessments Tell Us about the Threat Status of Fungi? *Diversity* **14**, 736 (2022).
19. Van Der Heijden, M. G. A., Martin, F. M., Selosse, M. & Sanders, I. R. Mycorrhizal ecology and evolution: the past, the present, and the future. *New Phytol.* **205**, 1406–1423 (2015).
20. Jetz, W., McGowan, J., Rinnan, D. S., Possingham, H. P., Visconti, P., O'Donnell, B. & Londoño-Murcia, M. C. Include biodiversity representation indicators in area-based conservation targets. *Nat. Ecol. Evol.* **6**, 123–126 (2021).
21. Guerra, C. A., Bardgett, R. D., Caon, L., Crowther, T. W., Delgado-Baquerizo, M., Montanarella, L., Navarro, L. M., Orgiazzi, A., Singh, B. K., Tedersoo, L., Vargas-Rojas, R., Briones, M. J. I., Buscot, F., Cameron, E. K., Cesarz, S., Chatzinotas, A., Cowan, D. A., Djukic, I., Van Den Hoogen, J., Lehmann, A., Maestre, F. T., Marín, C., Reitz, T., Rillig, M. C., Smith, L. C., De Vries, F. T., Weigelt, A., Wall, D. H. & Eisenhauer, N. Tracking, targeting, and conserving soil biodiversity. *Science* **371**, 239–241 (2021).

22. Větrovský, T., Morais, D., Kohout, P., Lepinay, C., Algora, C., Awokunle Hollá, S., Bahnmann, B. D., Bílohnědá, K., Brabcová, V., D'Alò, F., Human, Z. R., Jomura, M., Kolařík, M., Kvasničková, J., Lladó, S., López-Mondéjar, R., Martinović, T., Mašínová, T., Meszárošová, L., Michalčíková, L., Michalová, T., Mundra, S., Navrátilová, D., Odriozola, I., Piché-Choquette, S., Štursová, M., Švec, K., Tláskal, V., Urbanová, M., Vlk, L., Voříšková, J., Žifčáková, L. & Baldrian, P. GlobalFungi, a global database of fungal occurrences from high-throughput-sequencing metabarcoding studies. *Sci. Data* **7**, 228 (2020).
23. Nilsson, R. H., Larsson, K.-H., Taylor, A. F. S., Bengtsson-Palme, J., Jeppesen, T. S., Schigel, D., Kennedy, P., Picard, K., Glöckner, F. O. & Tedersoo, L. The UNITE database for molecular identification of fungi: handling dark taxa and parallel taxonomic classifications. *Nucleic Acids Res.* **47**, D259–D264 (2019).
24. Põlme, S., Abarenkov, K., Henrik Nilsson, R., Lindahl, B. D., Clemmensen, K. E., Kauserud, H., Nguyen, N., Kjøller, R., Bates, S. T., Baldrian, P., Frøslev, T. G., Adojaan, K., Vizzini, A., Suija, A., Pfister, D., Baral, H. O., Järv, H., Madrid, H., Nordén, J., Liu, J. K., Pawlowska, J., Põldmaa, K., Pärtel, K., Runnel, K., Hansen, K., Larsson, K. H., Hyde, K. D., Sandoval-Denis, M., Smith, M. E., Toome-Heller, M., Wijayawardene, N. N., Menolli, N., Reynolds, N. K., Drenkhan, R., Maharachchikumbura, S. S. N., Gibertoni, T. B., Læssøe, T., Davis, W., Tokarev, Y., Corrales, A., Soares, A. M., Agan, A., Machado, A. R., Argüelles-Moyao, A., Detheridge, A., de Meiras-Ottoni, A., Verbeken, A., Dutta, A. K., Cui, B. K., Pradeep, C. K., Marín, C., Stanton, D., Gohar, D., Wanasinghe, D. N., Otsing, E., Aslani, F., Griffith, G. W., Lumbsch, T. H., Grossart, H. P., Masigol, H., Timling, I., Hiiesalu, I., Oja, J., Kupagme, J. Y., Geml, J., Alvarez-Manjarrez, J., Ilves, K., Loit, K., Adamson, K., Nara, K., Küngas, K., Rojas-Jimenez, K., Bitenieks, K., Irinyi, L., Nagy, L. L., Soonvald, L., Zhou, L. W., Wagner, L., Aime, M. C., Öpik, M., Mujica, M. I., Metsoja, M., Ryberg, M., Vasar, M., Murata, M., Nelsen, M. P., Cleary, M., Samarakoon, M. C., Doilom, M., Bahram, M., Hagh-Doust, N., Dulya, O., Johnston, P., Kohout, P., Chen, Q., Tian, Q., Nandi, R., Amiri, R., Perera, R. H.,

dos Santos Chikowski, R., Mendes-Alvarenga, R. L., Garibay-Orijel, R., Gielen, R., Phookamsak, R., Jayawardena, R. S., Rahimlou, S., Karunarathna, S. C., Tibpromma, S., Brown, S. P., Sepp, S. K., Mundra, S., Luo, Z. H., Bose, T., Vahter, T., Netherway, T., Yang, T., May, T., Varga, T., Li, W., Coimbra, V. R. M., de Oliveira, V. R. T., de Lima, V. X., Mikryukov, V. S., Lu, Y., Matsuda, Y., Miyamoto, Y., Kõljalg, U. & Tedersoo, L. FungalTraits: a user-friendly traits database of fungi and fungus-like stramenopiles. *Fungal Divers.* **105**, (2020).

25. Větrovský, T., Kolařík ová, Z., Lepinay, C., Awokunle Hollá, S., Davison, J., Fleyberková, A., Gromyko, A., Jelínková, B., Kolařík, M., Krüger, M., Lejsková, R., Michalčíková, L., Michalová, T., Moora, M., Moravcová, A., Moulíková, Š., Odriozola, I., Öpik, M., Pappová, M., Piché-Choquette, S., Skřivánek, J., Vlk, L., Zobel, M., Baldrian, P. & Kohout, P. GlobalAMFungi: a global database of arbuscular mycorrhizal fungal occurrences from high-throughput sequencing metabarcoding studies. *New Phytol.* **240**, 2151–2163 (2023).
26. Öpik, M., Vanatoa, A., Vanatoa, E., Moora, M., Davison, J., Kalwij, J. M., Reier, Ü. & Zobel, M. The online database Maarj *AM* reveals global and ecosystemic distribution patterns in arbuscular mycorrhizal fungi (Glomeromycota). *New Phytol.* **188**, 223–241 (2010).
27. Ovaskainen, O. & Abrego, N. *Joint Species Distribution Modelling: With Applications in R*. (Cambridge University Press, 2020).
28. Tikhonov, G., Ovaskainen, O., Oksanen, J., de Jonge, M., Opedal, O. & Dallas, T. *Hmsc: Hierarchical Model of Species Communities*. https://github.com/hmsc-r/HMSC (2024).
29. Rahman, A. U., Tikhonov, G., Oksanen, J., Rossi, T. & Ovaskainen, O. Accelerating joint species distribution modelling with Hmsc-HPC by GPU porting. *PLOS Comput. Biol.* **20**, e1011914 (2024).
30. Karger, D. N., Conrad, O., Böhner, J., Kawohl, T., Kreft, H., Soria-Auza, R. W., Zimmermann, N. E., Linder, H. P. & Kessler, M. Climatologies at high resolution for the earth's land surface areas. *Sci. Data* **4**, 170122 (2017).

31. Karger, D. N., Conrad, O., Böhner, J., Kawohl, T., Kreft, H., Soria-Auza, R. W., Zimmermann, N. E., Linder, H. P. & Kessler, M. Climatologies at high resolution for the earth's land surface areas. EnviDat https://doi.org/10.16904/envidat.228 (2021).
32. Poggio, L., De Sousa, L. M., Batjes, N. H., Heuvelink, G., Kempen, B., Ribeiro, E. & Rossiter, D. SoilGrids 2.0: producing soil information for the globe with quantified spatial uncertainty. *Soil* **7**, 217–240 (2021).
33. McDowell, R. W., Noble, A., Pletnyakov, P. & Haygarth, P. M. A Global Database of Soil Plant Available Phosphorus. *Sci. Data* **10**, 125 (2023).
34. Spawn, S. A. & Gibbs, H. K. Global aboveground and belowground biomass carbon density maps for the year 2010. (2020) doi:10.3334/ORNLDAAC/1763.
35. Gorelick, N., Hancher, M., Dixon, M., Ilyushchenko, S., Thau, D. & Moore, R. Google earth engine: Planetary-scale geospatial analysis for everyone. *Remote Sens. Environ.* (2017) doi:10.1016/j.rse.2017.06.031.
36. Aybar, C. *Rgee: R Bindings for Calling the 'earth Engine' API*. https://CRAN.R-project.org/package=rgee (2023) doi:10.32614/CRAN.package.rgee.
37. Mammal Diversity Database. Mammal Diversity Database (Version 1.2). Zenodo https://doi.org/10.5281/zenodo.4139818 (2020).
38. Rodrigues, A. S. L., Andelman, S. J., Bakarr, M. I., Boitani, L., Brooks, T. M., Cowling, R. M., Fishpool, L. D. C., Da Fonseca, G. A. B., Gaston, K. J., Hoffmann, M., Long, J. S., Marquet, P. A., Pilgrim, J. D., Pressey, R. L., Schipper, J., Sechrest, W., Stuart, S. N., Underhill, L. G., Waller, R. W., Watts, M. E. J. & Yan, X. Effectiveness of the global protected area network in representing species diversity. *Nature* **428**, 640–643 (2004).
39. Dinerstein, E., Olson, D., Joshi, A., Vynne, C., Burgess, N. D., Wikramanayake, E., Hahn, N., Palminteri, S., Hedao, P., Noss, R., Hansen, M., Locke, H., Ellis, E. C., Jones, B., Barber, C. V., Hayes, R., Kormos, C., Martin, V., Crist, E., Sechrest, W., Price, L., Baillie, J. E. M., Weeden, D., Suckling, K., Davis, C., Sizer, N., Moore, R., Thau, D., Birch, T.,

Potapov, P., Turubanova, S., Tyukavina, A., De Souza, N., Pintea, L., Brito, J. C., Llewellyn, O. A., Miller, A. G., Patzelt, A., Ghazanfar, S. A., Timberlake, J., Klöser, H., Shennan-Farpón, Y., Kindt, R., Lillesø, J.-P. B., Van Breugel, P., Graudal, L., Voge, M., Al-Shammari, K. F. & Saleem, M. An Ecoregion-Based Approach to Protecting Half the Terrestrial Realm. *BioScience* **67**, 534–545 (2017).

40. Wijayawardene, N. N., Hyde, K. D., Al-Ani, L. K. T., Tedersoo, L., Haelewaters, D., Rajeshkumar, K. C., Zhao, R. L., Aptroot, A., Leontyev, D. V., Saxena, R. K., Tokarev, Y. S., Dai, D. Q., Letcher, P. M., Stephenson, S. L., Ertz, D., Lumbsch, H. T., Kukwa, M., Issi, I. V., Madrid, H., Phillips, A. J. L., Selbmann, L., Pfliegler, W. P., Horváth, E., Bensch, K., Kirk, P. M., Kolaríková, K., Raja, H. A., Radek, R., Papp, V., Dima, B., Ma, J., Malosso, E., Takamatsu, S., Rambold, G., Gannibal, P. B., Triebel, D., Gautam, A. K., Avasthi, S., Suetrong, S., Timdal, E., Fryar, S. C., Delgado, G., Réblová, M., Doilom, M., Dolatabadi, S., Pawlowska, J. Z., Humber, R. A., Kodsueb, R., Sánchez-Castro, I., Goto, B. T., Silva, D. K. A., de Souza, F. A., Oehl, F., da Silva, G. A., Silva, I. R., Blaszkowski, J., Jobim, K., Maia, L. C., Barbosa, F. R., Fiuza, P. O., Divakar, P. K., Shenoy, B. D. & Castañeda-Ruiz, R. F. Outline of Fungi and fungus-like taxa. *Mycosphere Online J. Fungal Biol.* **11**, 1060–1456 (2020).
41. Davison, J., Moora, M., Öpik, M., Adholeya, A., Ainsaar, L., Bâ, A., Burla, S., Diedhiou, A. G., Hiiesalu, I., Jairus, T., Johnson, N. C., Kane, A., Koorem, K., Kochar, M., Ndiaye, C., Pärtel, M., Reier, Ü., Saks, Ü., Singh, R., Vasar, M. & Zobel, M. Global assessment of arbuscular mycorrhizal fungus diversity reveals very low endemism. *Science* **349**, 970–973 (2015).
42. Bruns, T. D. & Taylor, J. W. Comment on 'Global assessment of arbuscular mycorrhizal fungus diversity reveals very low endemism'. *Science* **351**, 826 (2016).

43. Lutz, S., Mikryukov, V., Labouyrie, M., Bahram, M., Jones, A., Panagos, P., Delgado-Baquerizo, M., Maestre, F. T., Orgiazzi, A., Tedersoo, L. & van der Heijden, M. G. A. Global richness of arbuscular mycorrhizal fungi. *Fungal Ecol.* **74**, 101407 (2025).
44. Venter, O., Magrach, A., Outram, N., Klein, C. J., Possingham, H. P., Di Marco, M. & Watson, J. E. M. Bias in protected-area location and its effects on long-term aspirations of biodiversity conventions. *Conserv. Biol.* **32**, 127–134 (2018).
45. Wyborn, C. & Evans, M. C. Conservation needs to break free from global priority mapping. *Nat. Ecol. Evol.* **5**, 1322–1324 (2021).
46. Dahlberg, A. & Mueller, G. M. Applying IUCN red-listing criteria for assessing and reporting on the conservation status of fungal species. *Fungal Ecol.* **4**, 147–162 (2011).
47. Kivlin, S. N. Global mycorrhizal fungal range sizes vary within and among mycorrhizal guilds but are not correlated with dispersal traits. *J. Biogeogr.* **47**, 1994–2001 (2020).
48. Smith, J. R., Letten, A. D., Ke, P.-J., Anderson, C. B., Hendershot, J. N., Dhami, M. K., Dlott, G. A., Grainger, T. N., Howard, M. E., Morrison, B. M. L., Routh, D., San Juan, P. A., Mooney, H. A., Mordecai, E. A., Crowther, T. W. & Daily, G. C. A global test of ecoregions. *Nat. Ecol. Evol.* **2**, 1889–1896 (2018).
49. Delhaye, G., van der Linde, S., Bauman, D., Orme, C. D. L., Suz, L. M. & Bidartondo, M. I. Ectomycorrhizal fungi are influenced by ecoregion boundaries across Europe. *Glob. Ecol. Biogeogr.* **33**, e13837 (2024).
50. Lee-Yaw, J. A., McCune, J. L., Pironon, S. & Sheth, S. N. Species distribution models rarely predict the biology of real populations. *Ecography* **2022**, (2022).
51. Copoț, O., Lõhmus, A., Abarenkov, K., Tedersoo, L. & Runnel, K. Contribution of environmental DNA toward fungal Red Listing. *Front. Ecol. Environ.* **22**, e2791 (2024).
52. Massicotte, P. & South, A. *Rnaturalearth: World Map Data from Natural Earth*. https://CRAN.R-project.org/package=rnaturalearth (2023) doi:10.32614/CRAN.package.rnaturalearth.

53. Huang, T., Su, L.-J., Zeng, N.-K., Lee, S. M. L., Lee, S.-S., Thi, B. K., Zhang, W.-H., Ma, J., Huang, H.-Y., Jiang, S. & Tang, L.-P. Notes on Amanita section Validae in Hainan Island, China. *Front. Microbiol.* **13**, (2023).

Supplementary Information

Supplementary Text S1: Species distribution modeling, model evaluation, and prediction

We sourced AM fungal sequence data from GlobalAMFungi [1] and EcM fungal sequence data from GlobalFungi Release 5.0 (https://globalfungi.com/) [2].

The full GlobalAMFungi database contains 3,253 samples from 45 studies. These comprise sequences for 332 unique AM virtual taxa. We aggregated samples into "sites" according to their location within the same 30 arc-second (~1 km^2) grid cell and filtered to virtual taxa found in at least 31 sites. Our final AM fungal dataset contained 189 virtual taxa across 512 sites.

The full GlobalFungi Release 5.0 database contains 84,972 samples from 846 studies. When its sequences are clustered into operational taxonomic units (OTUs) at 97% similarity, classified according to the closest species hypothesis in UNITE version 10.0 [3], and filtered to known EcM genera according to FungalTraits [4], there remain 41,003 samples from 437 studies containing EcM fungi. We removed 2 Australian studies [5,6] previously identified as potentially problematic due to their unusually high number of unique OTUs [7]. We also removed all non-soil samples. This resulted in 27,740 soil samples from 435 studies, containing 92,458 unique EcM fungal OTUs. After aggregating samples into "sites" according to their location within the same 30 arc-second grid cell and filtering to OTUs found in at least 31 sites, we produced our final EcM fungal dataset containing 2,669 OTUs across 6,158 sites.

We used Hierarchical Modelling of Species Communities (HMSC) as implemented in the Hmsc *R* package [8] to model the distributions of AM fungal virtual taxa and EcM fungal OTUs. To describe our modeling choices, we provide an overview of the model structure here; more details are provided in HMSC reference material [9]. HMSC is a Bayesian species distribution modeling (SDM) framework based on generalized linear mixed models. For presence–absence data, the presence (y_{ij} = 1) or absence (y_{ij} = 0) of species *j* at site *i* is modeled as the response variable in a probit regression model with linear predictor L_{ij}.

$$y_{ij} \sim \text{Bernoulli}(\Phi(L_{ij}))$$

where Φ is the standard normal cumulative distribution function, also known in this context as the probit link function.

Given *n* sites and n_s species, we may write the $n \times n_s$ matrix containing elements *Lij* as **L**. **L** is modeled as the sum of fixed effects and random effects. The fixed-effect component $\mathbf{L}^F$ models the influence of the n_c environmental covariates on the probability of presence. n_c environmental covariates, denoted by the $n \times n_c$ matrix **X** (Table S1), on the probability of presence.

$$\mathbf{L} = \mathbf{L}^F + \mathbf{L}^R$$
$$\mathbf{L}^F = \mathbf{XB}$$

where **B** is the $n_c \times n_s$ matrix of coefficients describing species responses to environmental covariates and **X** is the $n \times n_c$ matrix of environmental covariates.

The random-effect component $\mathbf{L}^R$ models the influence of other processes not explicitly measured (e.g. dispersal limitation, missing environmental variables, and species interactions) on the probability of presence.

$$\mathbf{L}^R = \mathbf{H\Lambda}$$

The n_f latent factors, denoted by the $n \times n_f$ matrix **H**, are unobserved variables that attempt to capture spatial patterns in the data. (While HMSC accommodates hierarchical spatial designs, we use only one spatial scale; thus, our notation here differs somewhat from [9].) By default, the latent factors are modeled with a Gaussian process prior with an exponential covariance function $f(d) = \exp(-d/\alpha)$, where d is the distance between a given pair of sampling units and α is the spatial scale of autocorrelation inferred from the data. To overcome the high computational complexity associated with sampling-based inference of the Gaussian process for large datasets, [10] developed a computationally efficient approximation based on the Gaussian predictive process algorithm, which we employ in our models via the *Hmsc-hpc* Python package [11]. The species loadings, denoted by the n_f x n_s matrix **Λ**, capture species-specific associations with each latent factor. This capability of borrowing information between species makes HMSC a form of joint species distribution modeling (JSDM) [12].

To model the distributions of AM fungal virtual taxa, we fitted one HMSC model for the full set of taxa, creating a JSDM. We limited the maximum number of latent factors n_f to 10 to stay within memory constraints. For the Gaussian predictive process approximation, we constructed spatial knots at 20-degree increments in Euclidean coordinate space. We modified the prior distribution for α such that it retained a point density of 0.5 at its minimum value, $\alpha = 0$, and the remainder of its density declined linearly to zero at its maximum value, $\alpha = 15{,}000$ km. For the environmental covariates **X**, we extracted the mean values at each 30 arc-second grid cell in the World Geodetic System 1984 (WGS84) projection from the set of rasters described in Table S1 at each site location. We modified the prior distributions of the coefficients **B** as described in Table S1. We retained default priors for all other parameters. Based on inspection of Markov chain Monte Carlo (MCMC) chains judged to have adequate convergence, we ran the model with 2 chains, 100,000 burn-in iterations, and 100 samples with a thinning interval of 300 iterations.

To model the distributions of EcM fungal OTUs, we fitted one HMSC model for each taxon, creating a collection of independent SDMs rather than a JSDM. This was done after concluding that memory constraints prevented us from fitting a JSDM with sufficient latent factors to outperform independent SDMs, owing perhaps to the high degree of endemism in many EcM fungal taxa. The number of latent factors n_f in each SDM was thus limited to 1. For the Gaussian predictive process approximation, we constructed spatial knots at 15-degree increments in Euclidean coordinate space. We modified the prior distribution for α such that it retained a point density of 0.5 at its minimum value, $\alpha = 0$, and the remainder of its density was uniformly distributed between its minimum value and its maximum value, $\alpha = 10{,}000$ km. For the environmental covariates **X** and the coefficients **B**, we made the same modeling decisions described for AM fungi (Table S1). We retained default priors for all other parameters. Based on inspection of Markov chain Monte Carlo (MCMC) chains judged to have adequate convergence across a random sample of taxa, we ran each model with 2 chains, 100,000 burn-in iterations, and 100 samples with a thinning interval of 300 iterations.

To evaluate our models, we conducted nonspatial cross-validation across 5 folds of each guild's dataset. Due to computational limitations, cross-validation error is estimated using fewer Markov Chain Monte Carlo iterations than the full model (500 versus 1000) and may therefore underestimate performance. For EcM fungi, we conduct cross-validation using a randomly chosen subset of 20 OTUs to reduce computational demands, whereas we use the full set of AM fungal virtual taxa. In addition to a conventional error statistic, the area under the receiver–operator curve (AUC), we also report Tjur's R^2 (i.e., the coefficient of discrimination), as this metric is insensitive to the class imbalances characterizing sparse presence–absence datasets (Table S3).

While the *Hmsc* R package offers a function for making spatial predictions with fitted models, we encountered computational constraints when attempting to use it to create global kilometer-scale maps due to the complexity of calculating spatial latent factors. We then discovered that its spatial prediction algorithm is mathematically equivalent to kriging, and that Google Earth Engine offers an efficient kriging algorithm [13]. Thus, we translated *Hmsc*'s prediction algorithm into Google Earth Engine API calls via the *rgee* R package [14]. To further reduce the computational demand of kriging, we thinned the number of sites used as kriging points in the AM and EcM datasets such that at most one randomly selected site was included in each 200-km or 500-km Equal-Earth grid cell, respectively. We also limited the resolution of kriging to 50 km and the maximum kriging distance to 5,000 km. We used the same set of environmental rasters for prediction that we used for model fitting (Table S1), except that for each guild, we assumed constant sampling densities at the 86th percentile across sites. With these assumptions, we produced maps of the mean probability of presence at 1-km resolution for all AM and EcM fungal taxa.

Supplementary Text S2: Biome-level protection biases

To calculate the contribution of each biome's protected area network to each mycorrhizal fungal guild's global protection bias, we first propose that B_i can be decomposed into biome-level contributions B_{ij} such that

$$B_i = \text{sum}_j (B_{ij})$$

We define the range size weight W_{ij} as

$$W_{ij} = (a_{ij} / a_i) * \text{sqrt}(a_i) = a_{ij} / \text{sqrt}(a_i)$$

where a_{ij} is the range size of species i in biome j, in km^2.

We then assert that the decomposition is satisfied by

$$B_{ij} = W_{ij} * (p_{ij} - mu)$$

where p_{ij} is the proportion of the range of species i in biome j that is protected.

We note that given a biome j, B_{ij} are independently and identically distributed, ignoring phylogenetic dependence. We define the total cumulative contribution of biome j's protected area network to a guild's global protection bias as

$$B_j = \text{sum}_i (B_{ij})$$

Since each guild contains many species, B_j is approximately normally distributed with a standard error given by

$$\text{sqrt}(\text{sum}_i (W_{ij}) * \text{Var}(p_{ij}))$$

These statistics make it possible to test whether each biome's protected area network contributes positively or negatively to a given guild's global protection bias.

To quantify the proportion of bias explained by between-biome disparities in the proportion of area protected, we first define the following quantities:

$$TSS_{mu} = \text{sum}((W_{ij} * (p_{ij} - mu))^2)$$
$$ESS_{mu} = \text{sum}((W_{ij} * (mu_j - mu))^2)$$
$$RSS_{mu} = \text{sum}((W_{ij} * (p_{ij} - mu_j))^2)$$

where mu_j is the proportion protected of biome j.

These quantities are akin to total sum of squares, explained sum of squares, and residual sum of squares used in a regression context to calculate the proportion of total variance in the independent variable explained by the model. We modify that equation to calculate lower and upper bounds on the proportion of bias explained by between-biome disparities as:

$$R^2_{lower} = ESS_{mu} / (ESS_{mu} + RSS_{mu})$$
$$R^2_{upper} = ESS_{mu} / TSS_{mu}$$

Supplementary Tables

Table S1. Covariates used in the species distribution models.

Covariate	Data source	Reference(s)	Squared covariate included	Standardized mean of prior distribution of coefficient*	
				For linear covariate	For squared covariate, if included
Mean annual temperature, 1981-2010	CHELSA Bioclim Version 2.1	[15,16]	Yes	0	-4
Temperature range, 1981-2010			No	0	NA
Annual precipitation, 1981-2010			Yes	0	-4
Precipitation seasonality, 1981-2010			No	0	NA
Net primary production, 2022	NASA Land Processes DAAC MODIS/Terra Net Primary Production Version 6	(Running and Zhao 2019)	Yes	0	-4
Soil pH, 0-15 cm†	ISRIC SoilGrids 2.0	[17]	Yes	0	-4

Soil organic carbon content, 0-15 cm†			Yes	0	-4
Soil nitrogen content, 0-15 cm†			Yes	0	-4
Topsoil Olsen phosphorus content	See reference	[18]	Yes	0	-4
Aboveground biomass density, 2019-2021	ORNL DAAC GEDI L4B Gridded Aboveground Biomass Density, Version 2	[19]	Yes	0	-4
Natural log of sampling density‡	GlobalAMFungi / GlobalFungi Release 5	[1,2]	No	4	NA

* As a Bayesian modeling framework, Hierarchical Modelling of Species Communities requires prior distributions to be defined for each parameter. The values in this column show the means assumed for the prior distributions of the coefficients associated with each (centered and scaled) environmental covariate. Additionally, all prior distributions for the coefficients are assumed to have a standard deviation of 2.

† To estimate soil variables at 0-15 cm depth, we took the mean of the original data at 0-5 cm and 5-15 cm, weighted by thickness. Appropriate transformations were used to calculate the weighted mean pH.

‡ Sampling density is not given by raster data; it is operationalized at the site level as the total number of soil subsamples for AM fungi and the pooled number of amplicon reads for EcM fungi.

Table S2. Changes in key metrics as the probability cutoff defining the range of a species hypothesis increases.

Mycorrhizal fungal guild	Probability cutoff	Mean range size (km^2)	No. species hypotheses with zero range size	Naïve* mean proportion protected across ranges	Naïve* SD of proportion protected across ranges	Mean Species Protection Score	SD of Species Protection Score
Arbuscular mycorrhizal fungi	1%	56,884,952	0	0.160	0.020	97.9	3.59
	5%	40,127,323	0	0.157	0.026	95.5	6.61

	10%	31,381,426	0	0.155	0.027	94.5	7.86
	25%	19,257,681	0	0.151	0.034	90.7	11.1
Ectomycorrhizal fungi	1%	1,494,893	3	0.234	0.154	71.6	30.8
	5%	1,074,726	7	0.256	0.194	66.2	32.1
	10%	909,897	9	0.260	0.199	63.5	33.1
	25%	735,027	11	0.257	0.207	55.1	33.6

* The means and standard deviations (SD) are considered naïve because they are unweighted, whereas the means and SDs reported in the main text are weighted by the range-size weight, described in the Methods.

Table S3. Cross-validation summary statistics for species distribution models.

Mycorrhizal fungal guild	Area under the receiver operating characteristic curve (AUC), mean ± 1 SE	Tjur's R^2 (i.e., coefficient of discrimination), mean ± 1 SE
Arbuscular mycorrhizal fungi	0.839 ± 0.076	0.207 ± 0.083
Ectomycorrhizal fungi	0.755 ± 0.094	0.087 ± 0.051

Table S4. Species Protection Index (SPI) at the national level. 'NA' indicates that no predicted species ranges were contained within the country's borders so the SPI could not be calculated. Here, the SPI is calculated using the default curve, i.e. assuming that species with large range sizes require a 15% representation target.

Country	ISO 3166 country code	SPI	
		Arbuscular mycorrhizal fungi	Ectomycorrhizal fungi
Afghanistan	AFG	31.7	31.6
Angola	AGO	67.0	74.5
Albania	ALB	97.8	82.6
Andorra	AND	100.0	65.8
United Arab Emirates	ARE	85.4	81.7
Argentina	ARG	45.1	62.4
Armenia	ARM	100.0	86.2
Antigua and Barbuda	ATG	96.1	38.8
Australia	AUS	99.4	80.9
Austria	AUT	100.0	89.5
Azerbaijan	AZE	99.8	75.5
Burundi	BDI	43.1	15.3
Belgium	BEL	100.0	95.3
Benin	BEN	98.9	98.7

Burkina Faso	BFA	99.2	90.6
Bangladesh	BGD	8.7	10.0
Bulgaria	BGR	100.0	93.2
Bahrain	BHR	0.0	0.0
Bahamas	BHS	100.0	80.2
Bosnia and Herzegovina	BIH	76.6	49.1
Belarus	BLR	63.2	67.1
Belize	BLZ	99.5	95.9
Bolivia (Plurinational State of)	BOL	97.3	85.3
Brazil	BRA	94.8	73.9
Barbados	BRB	43.2	31.2
Brunei Darussalam	BRN	98.8	91.4
Bhutan	BTN	100.0	85.9
Botswana	BWA	97.5	91.5
Central African Republic	CAF	98.2	39.9
Canada	CAN	86.0	73.9
Chile	CHL	84.1	55.4
People's Republic of China	CHN	10.1	12.1
Côte d'Ivoire	CIV	100.0	99.9
Cameroon	CMR	73.6	33.0
Democratic Republic of the Congo	COD	94.2	69.7
Congo	COG	99.9	66.3
Colombia	COL	87.3	66.7
Comoros	COM	98.5	100.0
Cabo Verde	CPV	100.0	100.0
Costa Rica	CRI	100.0	92.3
Cuba	CUB	81.0	53.7
Cyprus	CYP	99.9	97.1
Czech Republic	CZE	99.5	86.6
Germany	DEU	100.0	96.3
Djibouti	DJI	14.1	15.3
Dominica	DMA	98.9	100.0
Denmark	DNK	100.0	94.1
Dominican Republic	DOM	99.9	99.5
Algeria	DZA	47.9	43.6
Ecuador	ECU	88.7	39.9
Egypt	EGY	28.3	13.5
Eritrea	ERI	88.3	45.2

Spain	ESP	100.0	90.2
Estonia	EST	99.9	68.4
Ethiopia	ETH	99.4	85.9
Finland	FIN	95.1	75.9
Fiji	FJI	21.7	33.0
France	FRA	100.0	84.0
Federated States of Micronesia	FSM	0.0	0.0
Gabon	GAB	99.9	65.5
United Kingdom	GBR	100.0	67.9
Georgia	GEO	97.2	66.3
Ghana	GHA	98.3	85.9
Guinea	GIN	99.1	100.0
Gambia	GMB	53.8	71.6
Guinea-Bissau	GNB	100.0	97.0
Equatorial Guinea	GNQ	97.0	57.8
Grenada	GRD	100.0	99.6
Greece	GRE	100.0	81.8
Greenland	GRL	NA	NA
Guatemala	GTM	99.2	63.2
Guyana	GUY	58.5	23.6
Honduras	HND	96.7	83.4
Croatia	HRV	100.0	87.8
Haiti	HTI	67.5	83.2
Hungary	HUN	100.0	98.1
Indonesia	IDN	66.4	67.4
India	IND	2.5	9.2
Ireland	IRL	98.9	52.7
Iran	IRN	34.8	32.9
Iraq	IRQ	37.1	67.5
Iceland	ISL	53.7	54.0
Israel	ISR	100.0	40.9
Italy	ITA	99.5	82.1
Jamaica	JAM	99.7	91.1
Jordan	JOR	60.9	42.3
Japan	JPN	99.8	73.3
Kazakhstan	KAZ	68.1	44.6
Kenya	KEN	99.6	93.2
Kyrgyzstan	KGZ	25.7	18.1
Cambodia	KHM	99.9	97.1

Kiribati	KIR	NA	NA
Saint Kitts and Nevis	KNA	NA	NA
Korea (Republic of)	KOR	100.0	87.6
Kuwait	KWT	99.7	100.0
Lao People's Democratic Republic	LAO	97.1	84.0
Lebanon	LBN	60.1	40.9
Liberia	LBR	71.5	43.8
Libya	LBY	0.0	0.0
Saint Lucia	LCA	100.0	100.0
Liechtenstein	LIE	100.0	93.6
Sri Lanka	LKA	100.0	78.9
Lesotho	LSO	97.2	85.6
Lithuania	LTU	99.2	71.1
Luxembourg	LUX	100.0	87.9
Latvia	LVA	99.3	57.3
Morocco	MAR	99.7	87.7
Monaco	MCO	NA	NA
Moldova	MDA	91.7	95.6
Madagascar	MDG	80.4	50.9
Maldives	MDV	NA	NA
Mexico	MEX	94.2	71.8
Marshall Islands	MHL	NA	NA
Republic of Macedonia	MKD	98.8	89.0
Mali	MLI	96.1	88.9
Malta	MLT	NA	NA
Myanmar	MMR	33.4	59.8
Montenegro	MNE	100.0	69.8
Mongolia	MNG	86.3	75.2
Mozambique	MOZ	99.8	97.5
Mauritania	MRT	1.8	12.6
Mauritius	MUS	68.7	76.3
Malawi	MWI	99.1	100.0
Malaysia	MYS	79.4	81.7
Namibia	NAM	97.8	99.6
Niger	NER	46.8	75.8
Nigeria	NGA	98.6	99.0
Nicaragua	NIC	99.9	99.2
Netherlands	NLD	100.0	82.8

Norway	NOR	98.9	51.2
Federal Democratic Republic of Nepal	NPL	93.6	51.5
Nauru	NRU	NA	NA
New Zealand	NZL	93.7	64.4
Oman	OMN	100.0	22.6
Pakistan	PAK	48.0	16.9
Panama	PAN	95.9	67.5
Peru	PER	91.8	50.4
Philippines	PHL	84.2	74.0
Palau	PLW	NA	NA
Papua New Guinea	PNG	35.2	8.2
Poland	POL	100.0	95.3
Korea (Democratic People's Republic of)	PRK	0.3	0.2
Portugal	PRT	100.0	76.0
Paraguay	PRY	92.7	69.6
Qatar	QAT	98.1	92.9
Romania	ROU	100.0	88.2
Russian Federation	RUS	66.0	63.0
Rwanda	RWA	52.2	49.6
Saudi Arabia	SAU	99.8	98.8
Sudan	SDN	9.2	8.3
Senegal	SEN	99.9	64.3
Singapore	SGP	84.6	55.0
Solomon Islands	SLB	7.5	6.3
Sierra Leone	SLE	96.9	86.8
El Salvador	SLV	99.8	95.4
San Marino	SMR	0.0	0.0
Somalia	SOM	0.1	1.5
Serbia	SRB	86.3	87.3
South Sudan	SSD	99.2	77.9
Sao Tome and Principe	STP	100.0	99.9
Suriname	SUR	99.5	80.8
Slovakia	SVK	100.0	97.7
Slovenia	SVN	100.0	94.0
Sweden	SWE	99.9	62.0
Swaziland	SWZ	98.2	57.7
Seychelles	SYC	100.0	100.0
Syrian Arab Republic	SYR	0.0	0.3

Chad	TCD	96.1	73.1
Togo	TGO	97.1	97.0
Thailand	THA	94.1	82.2
Tajikistan	TJK	56.0	52.8
Turkmenistan	TKM	30.9	38.0
Timor-Leste	TLS	93.2	87.4
Tonga	TON	30.5	23.1
Trinidad and Tobago	TTO	98.3	78.8
Tunisia	TUN	24.2	38.0
Turkey	TUR	1.2	1.2
Tuvalu	TUV	NA	NA
Taiwan, Province of China	TWN	67.2	68.0
Tanzania, United Republic of	TZA	100.0	95.5
Uganda	UGA	99.3	86.5
Ukraine	UKR	100.0	94.4
Uruguay	URY	51.2	67.0
United States	USA	66.5	69.5
Uzbekistan	UZB	46.6	47.8
Vatican City	VAT	NA	NA
Saint Vincent and Grenadines	VCT	99.3	100.0
Venezuela (Bolivarian Republic of)	VEN	100.0	97.4
Viet Nam	VNM	90.1	67.7
Vanuatu	VUT	23.0	17.4
Samoa	WSM	66.4	81.6
Yemen	YEM	30.7	6.3
South Africa	ZAF	79.5	58.2
Zambia	ZMB	100.0	92.1
Zimbabwe	ZWE	97.4	44.0
Kosovo	None	93.6	93.1

Table S5. Global protection biases of mycorrhizal fungi, including versus excluding croplands from the analysis.

Taxonomic group	Number of taxa analyzed	Croplands included in analysis?	Range- size-weighted mean (±1 SD) proportion protected	z †	P ‡
Arbuscular mycorrhizal fungi	189	Included	0.147 ± 0.033	-145	<0.001
		Excluded	0.168 ± 0.033	-27	<0.001
	2588	Included	0.180 ± 0.100	198	<0.001

Ectomycorrhizal fungi		Excluded	0.186 ± 0.103	338	<0.001

†,‡ These are the z-value and P-value, respectively, associated with the null hypothesis that the range- size-weighted mean is equal to the proportion protected of Earth's terrestrial surface (approximately 0.173), excluding Antarctica.

Supplementary Figures

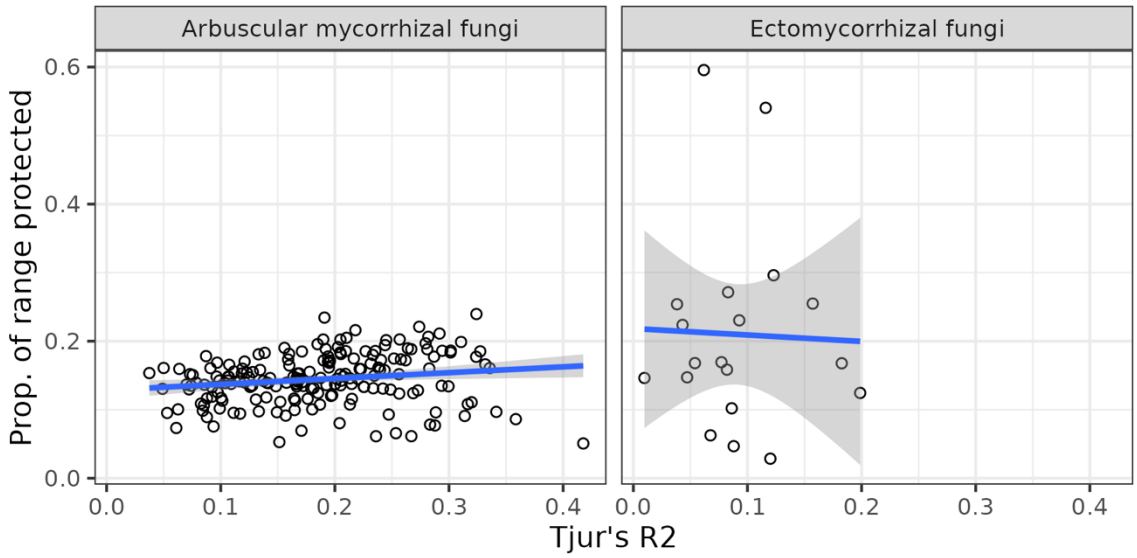

Figure S1. Performance of 20 randomly selected ectomycorrhizal fungal species distribution models versus the proportion protected of the predicted species range. Tjur's R^2 (i.e., the coefficient of discrimination) is derived from 5-fold cross-validation on the full set of presence–absence records for the 20 species.

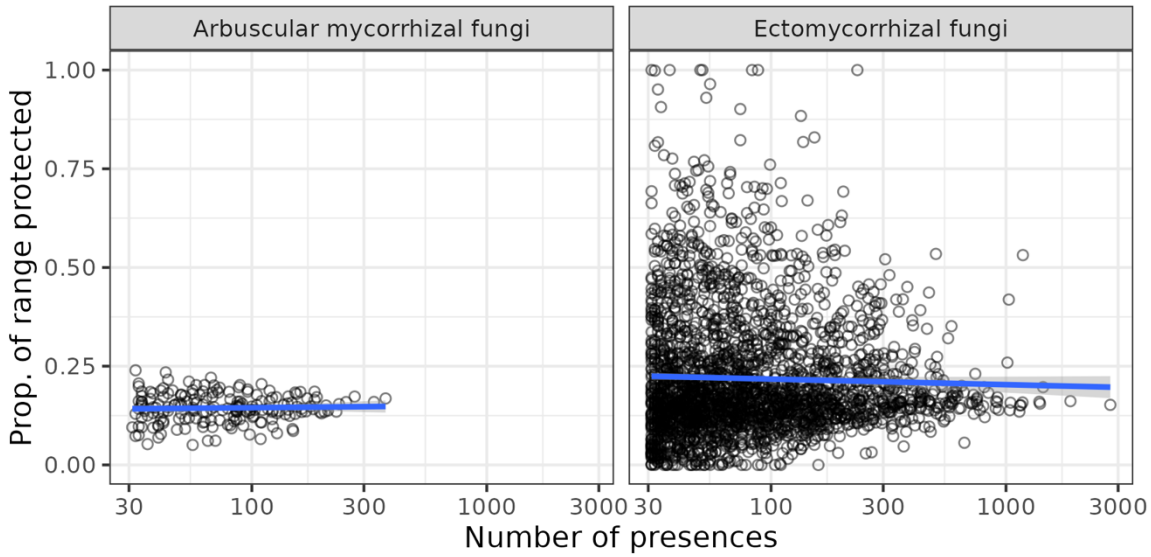

Figure S2. Number of presences of each species in the dataset versus the proportion protected of the predicted species range.

References

Running, S., and Zhao, M. (2019). *MOD17A3HGF MODIS/Terra Net Primary Production Gap-Filled Yearly L4 Global 500 m SIN Grid V006* [Data set]. NASA Land Processes Distributed Active Archive Center. https://doi.org/10.5067/MODIS/MOD17A3HGF.006 Date Accessed: 2025-07-13

1. Větrovský, T., Kolaříková, Z., Lepinay, C., Awokunle Hollá, S., Davison, J., Fleyberková, A., Gromyko, A., Jelínková, B., Kolařík, M., Krüger, M., Lejsková, R., Michalčíková, L., Michalová, T., Moora, M., Moravcová, A., Moulíková, Š., Odriozola, I., Öpik, M., Pappová, M., Piché-Choquette, S., Skřivánek, J., Vlk, L., Zobel, M., Baldrian, P. & Kohout, P. GlobalAMFungi: a global database of arbuscular mycorrhizal fungal occurrences from high-throughput sequencing metabarcoding studies. *New Phytol.* **240**, 2151–2163 (2023).
2. Větrovský, T., Morais, D., Kohout, P., Lepinay, C., Algora, C., Awokunle Hollá, S., Bahnmann, B. D., Bílohnědá, K., Brabcová, V., D'Alò, F., Human, Z. R., Jomura, M., Kolařík, M., Kvasničková, J., Lladó, S., López-Mondéjar, R., Martinović, T., Mašínová, T., Meszárošová, L., Michalčíková, L., Michalová, T., Mundra, S., Navrátilová, D., Odriozola, I., Piché-Choquette, S., Štursová, M., Švec, K., Tláskal, V., Urbanová, M., Vlk, L., Voříšková, J., Žifčáková, L. & Baldrian, P. GlobalFungi, a global database of fungal occurrences from high-throughput-sequencing metabarcoding studies. *Sci. Data* **7**, 228 (2020).
3. Nilsson, R. H., Larsson, K.-H., Taylor, A. F. S., Bengtsson-Palme, J., Jeppesen, T. S., Schigel, D., Kennedy, P., Picard, K., Glöckner, F. O. & Tedersoo, L. The UNITE

database for molecular identification of fungi: handling dark taxa and parallel taxonomic classifications. *Nucleic Acids Res.* **47**, D259–D264 (2019).

4. Põlme, S., Abarenkov, K., Henrik Nilsson, R., Lindahl, B. D., Clemmensen, K. E., Kauserud, H., Nguyen, N., Kjøller, R., Bates, S. T., Baldrian, P., Frøslev, T. G., Adojaan, K., Vizzini, A., Suija, A., Pfister, D., Baral, H. O., Järv, H., Madrid, H., Nordén, J., Liu, J. K., Pawlowska, J., Põldmaa, K., Pärtel, K., Runnel, K., Hansen, K., Larsson, K. H., Hyde, K. D., Sandoval-Denis, M., Smith, M. E., Toome-Heller, M., Wijayawardene, N. N., Menolli, N., Reynolds, N. K., Drenkhan, R., Maharachchikumbura, S. S. N., Gibertoni, T. B., Læssøe, T., Davis, W., Tokarev, Y., Corrales, A., Soares, A. M., Agan, A., Machado, A. R., Argüelles-Moyao, A., Detheridge, A., de Meiras-Ottoni, A., Verbeken, A., Dutta, A. K., Cui, B. K., Pradeep, C. K., Marín, C., Stanton, D., Gohar, D., Wanasinghe, D. N., Otsing, E., Aslani, F., Griffith, G. W., Lumbsch, T. H., Grossart, H. P., Masigol, H., Timling, I., Hiiesalu, I., Oja, J., Kupagme, J. Y., Geml, J., Alvarez-Manjarrez, J., Ilves, K., Loit, K., Adamson, K., Nara, K., Küngas, K., Rojas-Jimenez, K., Bitenieks, K., Irinyi, L., Nagy, L. L., Soonvald, L., Zhou, L. W., Wagner, L., Aime, M. C., Öpik, M., Mujica, M. I., Metsoja, M., Ryberg, M., Vasar, M., Murata, M., Nelsen, M. P., Cleary, M., Samarakoon, M. C., Doilom, M., Bahram, M., Hagh-Doust, N., Dulya, O., Johnston, P., Kohout, P., Chen, Q., Tian, Q., Nandi, R., Amiri, R., Perera, R. H., dos Santos Chikowski, R., Mendes-Alvarenga, R. L., Garibay-Orijel, R., Gielen, R., Phookamsak, R., Jayawardena, R. S., Rahimlou, S., Karunarathna, S. C., Tibpromma, S., Brown, S. P., Sepp, S. K., Mundra, S., Luo, Z. H., Bose, T., Vahter, T., Netherway, T., Yang, T., May, T., Varga, T., Li, W., Coimbra, V. R. M., de

Oliveira, V. R. T., de Lima, V. X., Mikryukov, V. S., Lu, Y., Matsuda, Y., Miyamoto, Y., Kõljalg, U. & Tedersoo, L. FungalTraits: a user-friendly traits database of fungi and fungus-like stramenopiles. *Fungal Divers.* **105**, (2020).

5. Bissett, A., Fitzgerald, A., Meintjes, T., Mele, P. M., Reith, F., Dennis, P. G., Breed, M. F., Brown, B., Brown, M. V., Brugger, J., & others. Introducing BASE: the biomes of australian soil environments soil microbial diversity database. *GigaScience* **5**, 21 (2016).
6. Yan, D., Mills, J. G., Gellie, N. J., Bissett, A., Lowe, A. J. & Breed, M. F. High-throughput eDNA monitoring of fungi to track functional recovery in ecological restoration. *Biol. Conserv.* **217**, 113–120 (2018).
7. Van Nuland, M. E., Averill, C., Stewart, J. D., Prylutskyi, O., Corrales, A., van Galen, L. G., Manley, B. F., Qin, C., Lauber, T., Mikryukov, V., Dulia, O., Furci, G., Marín, C., Sheldrake, M., Weedon, J. T., Peay, K. G., Cornwallis, C. K., Větrovský, T., Kohout, P., Baldrian, P., Tedersoo, L., West, S. A., Crowther, T. W., Kiers, E. T. & van den Hoogen, J. Global hotspots of mycorrhizal fungal richness are poorly protected. *Nature* 1–9 (2025) doi:10.1038/s41586-025-09277-4.
8. Tikhonov, G., Ovaskainen, O., Oksanen, J., de Jonge, M., Opedal, O. & Dallas, T. *Hmsc: Hierarchical Model of Species Communities*. https://github.com/hmsc-r/HMSC (2024).
9. Ovaskainen, O. & Abrego, N. *Joint Species Distribution Modelling: With Applications in R*. (Cambridge University Press, 2020).

10. Tikhonov, G., Duan, L., Abrego, N., Newell, G., White, M., Dunson, D. & Ovaskainen, O. Computationally efficient joint species distribution modeling of big spatial data. *Ecology* **101**, 1–8 (2020).
11. Rahman, A. U., Tikhonov, G., Oksanen, J., Rossi, T. & Ovaskainen, O. Accelerating joint species distribution modelling with Hmsc-HPC by GPU porting. *PLOS Comput. Biol.* **20**, e1011914 (2024).
12. Warton, D. I., Blanchet, F. G., O'Hara, R. B., Ovaskainen, O., Taskinen, S., Walker, S. C. & Hui, F. K. C. So Many Variables: Joint Modeling in Community Ecology. *Trends Ecol. Evol.* **30**, 766–779 (2015).
13. Gorelick, N., Hancher, M., Dixon, M., Ilyushchenko, S., Thau, D. & Moore, R. Google earth engine: Planetary-scale geospatial analysis for everyone. *Remote Sens. Environ.* (2017) doi:10.1016/j.rse.2017.06.031.
14. Aybar, C. *Rgee: R Bindings for Calling the 'earth Engine' API*. https://CRAN.R-project.org/package=rgee (2023) doi:10.32614/CRAN.package.rgee.
15. Karger, D. N., Conrad, O., Böhner, J., Kawohl, T., Kreft, H., Soria-Auza, R. W., Zimmermann, N. E., Linder, H. P. & Kessler, M. Climatologies at high resolution for the earth's land surface areas. *Sci. Data* **4**, 170122 (2017).
16. Karger, D. N., Conrad, O., Böhner, J., Kawohl, T., Kreft, H., Soria-Auza, R. W., Zimmermann, N. E., Linder, H. P. & Kessler, M. Climatologies at high resolution for the earth's land surface areas. EnviDat https://doi.org/10.16904/envidat.228 (2021).
17. Poggio, L., De Sousa, L. M., Batjes, N. H., Heuvelink, G., Kempen, B., Ribeiro, E. & Rossiter, D. SoilGrids 2.0: producing soil information for the globe with quantified spatial uncertainty. *Soil* **7**, 217–240 (2021).

18. McDowell, R. W., Noble, A., Pletnyakov, P. & Haygarth, P. M. A Global Database of Soil Plant Available Phosphorus. *Sci. Data* **10**, 125 (2023).
19. Spawn, S. A. & Gibbs, H. K. Global aboveground and belowground biomass carbon density maps for the year 2010. (2020) doi:10.3334/ORNLDAAC/1763.